BioMetals (2006) 19:437–450
DOI 10.1007/s10534-005-4576-y

Tracing of labile zinc in live fish hepatocytes using FluoZin-3

Frederik A. R. Muylle[1,*], Dirk Adriaensen[2], Wim De Coen[1], Jean-Pierre Timmermans[2] & Ronny Blust[1]
[1]*Department of Biology, University of Antwerp, Groenenborgerlaan 171, B-2020, Antwerp, Belgium;* [2]*Department of Biomedical Sciences, University of Antwerp, Groenenborgerlaan 171, B-2020, Antwerp, Belgium; *Author for correspondence (Tel.: +32-32653482; Fax: +32-32653497; E-mail: frederik.muylle@diabetes-vdv.be)*

Received 11 September 2005; accepted 24 October 2005

Key words: chelatable zinc, fluorescent zinc probe, confocal zinc imaging, rainbow trout hepatocyte, FluoZin-3

Abstract

Intracellular zinc levels are homeostatically regulated and although most is bound, a pool of labile Zn(II) is present in cells. We show here that the zinc probe FluoZin-3 is useful to monitor zinc fluxes during fluorescent imaging of the trout hepatic cell line D11. Nuclei and bulk cytosol appeared to lack detectable labile zinc, while the punctuate staining pattern colocalized with a lysosome-specific probe. Applying extracellular zinc alone resulted in vesicular sequestration of the metal ion. Together with Na-pyrithione a delayed and toxic rise in cellular fluorescence was triggered. When using another ionophore, 4-Br A23187, a zinc buffering effect of the vesicular pools was evident. Secondly, *N*-ethylmaleimide induced a homogeneous fluorescence rise, which was strongly enhanced by addition of Zn-pyrithione and disappeared after TPEN washing. This suggests the involvement of thiol residues in controlling available cytosolic zinc. Our observations have implications for the interpretation of calculated intracellular Zn^{2+} concentrations.

Introduction

Zinc is an essential element, which regulates a plethora of cellular processes, such as enzymatic activity, cell division, transcription, neurotransmission and apoptosis (Vallee & Falchuk 1993; Salguiero *et al.* 2000). But as a result of human activity, zinc and other metals are also important contaminants of the aquatic environment. Freshwater fish, which can use either ingested food or water as sources, take up these metals and process them (Bury *et al.* 2003). High levels can result in toxicity or acclimation, depending on the exposure regime (Hogstrand & Wood 1995; Alsop & Wood 2000). Cellular mechanisms behind these phenomena are not well understood. Investigating zinc regulation at the cellular level is crucial to ultimately understand the consequences of its disturbance. Generally, inside eukaryotic cells Zn^{2+} is bound relatively strongly to ligands such as amino acids (cysteine, histidine), reduced glutathione (GSH) (Krezel *et al.* 2003), metalloproteins and metallothionein-like proteins (MTs). The latter are small (6–10 kDa) cysteine-rich proteins, thought to be involved in maintaining basal zinc levels and detoxification of non-essential metals (Kägi 1991). Considering the high affinity of many of these binding sites (e.g. $K_d \sim 10^{-13}$ for metallothionein at pH 7) , theoretical calculations suggest that the resulting free Zn^{2+} activity in the cellular environment must be extremely low (picomolar or lower), which is confirmed by an apparent ultrasensitivity of the Zn(II) sensing factors involved in bacterial zinc metabolism (Outten & O'Halloran 2001). Recent research on eukaryotic zinc regulation (Gaither & Eide 2001) has pointed out that shuttling of zinc across intracellular compartments or zinc exchange with

the extracellular fluid occurs through the action of transporters of the ZIP (Zrt, Irt-like protein) or CDF (Cation Diffusion Facilitator) families, responsible for cytoplasmic influx and efflux (or sequestration), respectively. An excellent review on mammalian zinc transporters was provided by Kambe and co-workers (Kambe *et al.* 2004). Generally, the ZnT-type (CDF) zinc transporters appear important to physically discharge cytoplasmic zinc loads by facilitating subcellular (vesicular) sequestration or zinc export. Both membrane associated transporters and mobile ligands such as MTs probably contribute to the overall zinc homeostasis and protection against toxicity. However, their relative physiological role remains to be established.

Rainbow trout (*Oncorhynchus mykiss*) is a freshwater fish species whose physiology has long been investigated in terms of metal toxicology and acclimation. In trout, hepatic metallothioneins are involved in the response to metal exposure (Ley *et al.* 1983) but other zinc-binding proteins have been invoked to contribute to normal metal homeostasis (Pierson 1985). Finally, zinc transport systems corresponding to their mammalian counterparts were found in fish cells (Qiu *et al.* 2005). Since the fish liver is considered as a central unit for processing of intestinally absorbed metals and redistribution to other body compartments (Hogstrand & Wood 1996), studying hepatocytes is fundamental to gain understanding of zinc regulation in the whole organism. Several destructive methods have been employed to trace vesicular Zn in tissues (Lopez-Garcia *et al.* 2002; Sauer & Watabe 1989; Frederickson *et al.* 1987), but non-destructive analytical tools are required to monitor cellular Zn (II) dynamics *in situ*. Fluorescent probing of Zn (II) ions (or more precisely defined "chelatable zinc") is such an approach. Previously, the fluorescent zinc probe TSQ (toluene sulphonamide quinoline) and the related sensor Zinquin were used to measure available zinc in freshly isolated trout hepatocytes (Gagné & Blaise 1996) or primary rat hepatocytes (Brand & Kleineke 1996), respectively. However, in these reports, no information was provided concerning the subcellular fluorescence distribution. Although quite zinc-selective, both quinoline-based sensors lack a straightforward stoechiometry of their zinc complexes and Zinquin seems to chelate some zinc bound as metallothionein (MT) *in vitro* (Coyle *et al.* 1994). Nonetheless, Zinquin staining has been imaged for a large number of mammalian cell types and a reoccurring theme is its punctuate appearance (Nasir *et al.* 1999; Zalewski *et al.* 1993), observed both in continuous cell lines and primary cells (Tang *et al.* 2002), at least suggesting relevance to the *in vivo* zinc physiology. This fluorescence pattern was previously explained by its co-localization with ZnT-2 to a late endosomal compartment in Zn-exposed BHK cells (Palmiter *et al.* 1996a). Furthermore, punctiform Zinquin fluorescence has been attributed to the presence of ZnT-3 in synaptic vesicles (Palmiter *et al.* 1996b), but colocalization with ZnT-4 could not be confirmed in MDCK cells (Ranaldi *et al.* 2002) or human breast epithelial cells (Michalczyk *et al.* 2002). Recently, Haase & Beyersmann (2002) provided the first clear evidence that cellular fluorescence patterns of Zinquin are dynamic and associated with true zinc fluxes in C6 glioma cells. Clearly, fluorescent zinc sensors may help to reveal the function of zinc transporting mechanisms in particular cell types. In our work we searched for a probe with desirable properties for confocal fluorescence imaging, namely good sensitivity, visible wavelength absorption, and a high, zinc-selective response. In this perspective, we have considered fluorescent imaging of D11 trout hepatocytes loaded with the fluorescent zinc probe FluoZin-3 to be a promising approach.

As reported here, we first identified subcellular areas of high zinc activity in normal proliferating D11 cells using different zinc sensors. Secondly, we tested the ability of FluoZin-3 to sense the subcellular dynamics of available zinc in simple zinc flux models: (1) exogenous zinc uptake, (2) exogenous zinc together with an ionophore to induce cytosolic metal overload and finally (3) zinc release from endogenous binding sites. Starting from these approaches we discuss how to critically interpret calculated free zinc levels after calibration procedures.

Materials and methods

Chemicals and reagents

Tissue culture grade media were obtained from Invitrogen Life Technologies (Paisley, Scotland, UK). Cell culture flasks were from Nunc (Wiesbaden, Germany). FluoZin-3 AM, BTC-5N AM,

TPEN (*N*,*N*,*N*′,*N*′-tetrakis(2-pyridyl-methyl)ethylenediamine), LysoTracker Red DND99 and MitoTracker Deep Red were purchased from Molecular Probes (Leiden, the Netherlands) and kept frozen (−20 °C) as DMSO stock solutions. ZinPyr-1 (dissolved in DMSO) was synthesized by a Mannich reaction under reflux heating as summarized in Burdette *et al*. (2001). Na-pyrithione and 4-Br-calcimycin were from Sigma (St. Louis, MO, USA). All salts, buffers and BSA (bovine serum albumin, fraction V) were obtained from the same manufacturer (Merck, Darmstadt, Germany) unless otherwise stated.

Cell culture

D11 cells (DSMZ, Braunschweig, Germany) (passage 10–20) were grown in 75 cm^2 flasks, using L-15 medium, supplemented with L-glutamine (2 mg/ml), PenStrep (penicillin 100 U/ml, streptomycin 100 μg/ml) and 10% heat-inactivated FBS (foetal bovine serum) . D11 is a fast-growing subclone derived from fibroblastic R1 cells (Ahne, 1985). Cells were routinely subcultured every 4 to 5 days at a 1:3 ratio. Incubation was at 22 °C in a humidified cell culture chamber. For confocal microscopy experiments, cells were seeded 24 h in advance at $\pm 7.5\times10^4$ cells/cm^2 on acid/ethanol washed and heat sterilized glass no. 1 coverslips (PeCon, Erbach, Germany). In this way, subconfluent ($\pm$70–80%) cells were obtained on the day of experimentation.

Labelling of cells

Subconfluent cell layers of D11 were incubated in L-15 phosphate-buffered salt solution (L-15 PBS) consisting of (in mM): 136.9 NaCl, 5.3 KCl, 1.34 Na_2HPO_4, 0.44 KH_2PO_4, 1.26 $CaCl_2$, 0.99 $MgCl_2{\cdot}7H_2O$, 0.81 $MgSO_4{\cdot}7H_2O$, 5 D-galactose, 0.2% BSA, pH 7.4 at constant room temperature (22 ± 1°C). Specific fluorescent probes were added to this medium at the following concentrations and for respective incubation times before confocal imaging of D11 cells: (1) *zinc indicators*: FluoZin-3 AM (5 μM, 45 min); BTC-5N AM (5 μM, 30 min); ZinPyr-1 (5 μM, 20 min). Before final dilution in the incubation buffer, AM ester probes, dissolved in DMSO, were mixed 1:1 with Pluronic acid (20% in DMSO) to improve dispersion in the aqueous media. (2) *organelle tracers*: LysoTracker Red DND99 (50 nM, 15 min) and MitoTracker Deep Red (50 nM, 1–2 min). Subsequently, cells were rinsed once with probe-free incubation buffer and imaging was initiated immediately thereafter.

Confocal microscopy

D11 cells cultured on glass coverslips were placed inside a culture chamber and maintained at 21–22 °C. A Zeiss LSM510 confocal laser scanning set-up operated by LSM5 software (Zeiss, Jena, Germany) was employed to acquire fluorescent images using a 63× C-Apochromat (numerical aperture 1.2, water immersion) or a 25× Plan-Neofluor (numerical aperture 0.8, immersion corrected) objective. Pinholes of the confocal configuration were set at 0.667 μm giving optical cell slices of about 5 μm thickness. Excitation of FluoZin-3 with a 488 nm Ar laser line was only at 1–2% of the maximum laser power output (25 mW), in order to reduce photobleaching significantly. For fluorescence detection, a 495 nm beamsplitter and a 500–530 nm bandpass filter were used. This filter set combination was also used for imaging of ZinPyr-1. BTC-5N was excited with the 458 nm Ar laser line and imaged using the same fluorescence emission filters. In FluoZin-3 or ZinPyr-1 emission filter set combinations, the same excitation beam splitter (UV/488/543/633) was used. In case of BTC-5N, a 488/514 beam splitter was inserted after the excitation beam. For co-localization experiments with organelle probes, a multitrack configuration was used which consisted of any of the described zinc probe configurations combined with LysoTracker Red DND99 (HeNe excitation 543 nm, emission band-pass filter 565–615 nm) and MitoTracker Deep Red (HeNe excitation: 633 nm, emission: 650 nm long-pass filter) settings. In preliminary experiments, excitation intensities and detector gain were optimized to rule out green (<550 nm) and red (>550 nm) detection channel cross-talk. Additionally, the lack of interfering autofluorescence of D11 cells was confirmed for each of the configurations used. While performing kinetic measurements with FluoZin-3, time series of 8-bit images (512×512 pixels) of a cell field were recorded and stored as LSM format files. For *post-hoc*

intensity analysis, ImageJ version 1.27z (National Institutes of Health, Bethesda, USA) was used in combination with a Zeiss LSM plug-in.

Microplate spectrofluorimetry

A Spectramax Gemini fluorescent microplate reader (Molecular Devices, Oregon, USA) was operated with the Softmax Pro 3.1.1. software interface. Zinc probes were diluted in a simplified cytosol-like medium (high K^+, low Na^+) buffered with MOPS at pH 7.2 . To these working solutions, different metal salts were added from 100 mM aqueous stocks. An 100 μl aliquot was transferred to a black microtiter plate (Greiner Bio-one, Frickhausen, Germany) and wells were scanned for fluorescence using these respective parameters for excitation, cut-off and emission wavelengths of the different probes: 488-515-530 (ZinPyr-1, FluoZin-3); 415-470-520 (BTC-5N).

Zinc exposure experiments

Before extracellular zinc exposure, D11 cells were loaded with 5 μM FluoZin-3 AM, washed once and subjected to a short equilibration (10 min) in nominally zinc-free incubation buffer to complete probe de-esterification and to obtain a stable fluorescence signal. Next, cells were exposed to 10 μM nominal $ZnCl_2$ in HEPES-buffered L-15 salt solution (phosphate free and without added bicarbonate) consisting of (in mM): 136.9 NaCl, 5.3 KCl, 1.26 $CaCl_2$, 0.99 $MgCl_2{\cdot}7H_2O$, 0.81 $MgSO_4{\cdot}7H_2O$, 5 D-galactose, 10 mM Na-HEPES, pH 7.4. $ZnCl_2$ was added from a 10 times concentrated stock in the same buffer. Cells were imaged for 15 min after triggering with zinc. In order to permeabilize cells for Zn^{2+} with or without pretreatment with 10 μM $ZnCl_2$, the medium was switched to Ca^{2+} and Mg^{2+} free HEPES buffer consisting of (in mM): 141 NaCl, 5.3 KCl, 5 D-galactose, 10 mM Na-HEPES, pH 7.4. In addition, this solution contained 10 μM $ZnCl_2$ together with either 10 μM sodium pyrithione or 1 μM 4-Br A23187 as ionophores. For long-term Zn-pyrithione exposure, the fluorescence of a selected homogeneous cell field (consisting of ± 25 cells) was recorded up to 120 min with a maximal frequency of 2 min^{-1} and eventually adjusted down to 1/10 min.

Zinc release experiments

NEM (*N*-ethylmaleimide) was used as a potent blocker of sulfhydryl groups to release zinc complexed by thiolate residues such as cystein, glutathione or as present in metallothionein. A 500 times concentrated stock solution of NEM in ethanol (stored at −20 °C) was freshly diluted to 1 mM in L-15 HEPES buffer before use. After equilibration of D11 cells in 1.8 ml buffer, 200 μl of this NEM working solution was quickly added to obtain a final concentration of 100 μM NEM. Confocal images were recorded every 30 seconds for a period of 30 min thereafter. After this time the medium was carefully removed and replaced with 10 μM Zn-pyrithione in Ca^{2+} and Mg^{2+} free HEPES buffer. Cellular fluorescence was then imaged until a stable fluorescence level was obtained. At this point the medium was switched to 50 μM TPEN, a membrane permeable heavy metal chelator. Addition of TPEN allows to sequester all Zn^{2+} complexed with the fluorescent probe until a baseline signal of unbound probe is reached (Arslan *et al*. 1985).

Quantification of intracellular [Zn^{2+}] from FluoZin-3 experiments

To convert observed fluorescence changes to quantitative [Zn^{2+}] responses, the standard Grynckiewicz equation for non-ratiometric ion probes was applied (Grynkiewicz *et al*. 1985): $[Zn^{2+}] = K_d^*(F-F_{min})/(F_{max}-F)$ where F represents *integrated cellular fluorescence*, F_{min} the *minimum signal* obtained after TPEN treatment and F_{max} the *maximum* induced by Zn-pyrithione. At the end of $ZnCl_2$ or NEM exposures, such ionophore calibration procedures were performed. *Post-hoc* image analysis was performed on single cells selected for fluorescence intensity measurements (a total of 20–25 cells were used in each of 3 independent preparations).

Results

Characteristics of different zinc probe candidates in salt solution

To assess whether fluorescence patterns of zinc sensor loaded cells are related to probe

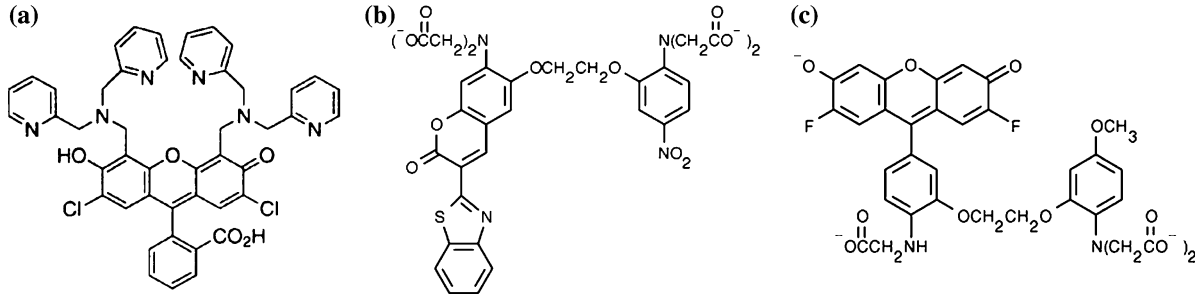

Figure 1. Molecular structures of ZinPyr-1, BTC-5N and FluoZin-3. (a) ZinPyr-1 (b) BTC-5N-AM (c) Fluozin-3-AM.

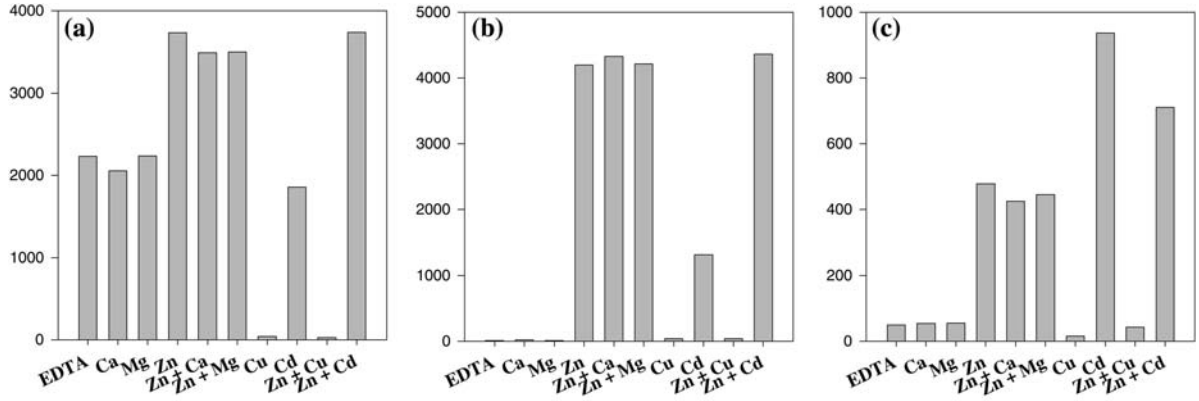

Figure 2. Response of ZinPyr-1, FluoZin-3 or BTC-5N to different divalent metal cations. (a) ZinPyr-1 5 μM; (b) FluoZin-3 0.35 μM; (c) BTC-5N 1 μM. Fluorescence data was measured in 120 mM KCl, 15 mM NaCl, 10 mM MOPS, pH 7.2. Test solutions were prepared in this medium with the following additions, respectively (as indicated under bars): Na_2EDTA 100 μM, $CaCl_2$ 100 μM + TPEN 50μM, $MgCl_2$ 1 mM + TPEN 50μM, $ZnCl_2$ 5 μM, $ZnCl_2$ 5 μM + $CaCl_2$ 100 μM, $ZnCl_2$ 5 μM + $MgCl_2$ 1 mM, $CuCl_2$ 5 μM, $CdCl_2$ 5 μM, $ZnCl_2$ 5 μM + $CuCl_2$ 5 μM, $ZnCl_2$ 5 μM + $CdCl_2$ 5 μM. Excitation-emission settings were as follows: ZinPyr-1 (488-530), FluoZin-3 (488-530), BTC-5N (415–520) (c). Y-axes represent relative fluorescence units.

particularities or represent a true labile zinc distribution pattern, three chemically different fluorescent zinc indicators were evaluated (Figure 1) in the D11 cell line. Whereas the monocarboxylic ZinPyr-1 1 (Burdette *et al.* 2001) is taken up as such, the other two tested probes (BTC-5N and FluoZin-3) are acetoxymethyl esterified and thus depend on cellular esterase to become active sensors (Haugland 2002). Figure 2 demonstrates that all three probes share a good specificity for heavy metals in the presence of Ca^{2+} or Mg^{2+} in a simplified cytosol-like salt medium. Cu^{2+} seems to quench the fluorescence of the zinc sensors, but it is unlikely that this species is abundant in a reducing intracellular environment. Apparent zinc affinity constants for ZinPyr-1, FluoZin-3 and BTC-5N were reported to be about 2 nM, 15 nM and 0.2 μM, respectively (Burdette *et al.* 2001; Haugland 2002) at high K^+ (50–100 mM) and neutral pH (MOPS buffer). FluoZin-3 clearly shows the highest fluorescence induction upon Zn^{2+} binding (Figure 2b) (> 100-fold).

Identification of lysosomes as pools of labile Zn(II) in D11 cells

Generally, after labelling of growing D11 cells with either one of the zinc probes, the nucleus and the bulk cytoplasmic space lack fluorescence, indicating the absence of a labile Zn^{2+} fraction in these compartments (Figure 3). Instead, cells typically showed a ''starry sky'' pattern distributed throughout the cytosol. To investigate whether the observed punctiform pools are associated with any known subcellular structure, we labelled D11 cells specifically for acidic environments (endosomal-lysosomal) with LysoTracker Red, or for mitochondrial compartments using MitoTracker Deep Red. In addition, we loaded cells with the zinc probes FluoZin-3-AM, ZinPyr-1 or BTC-5N-AM

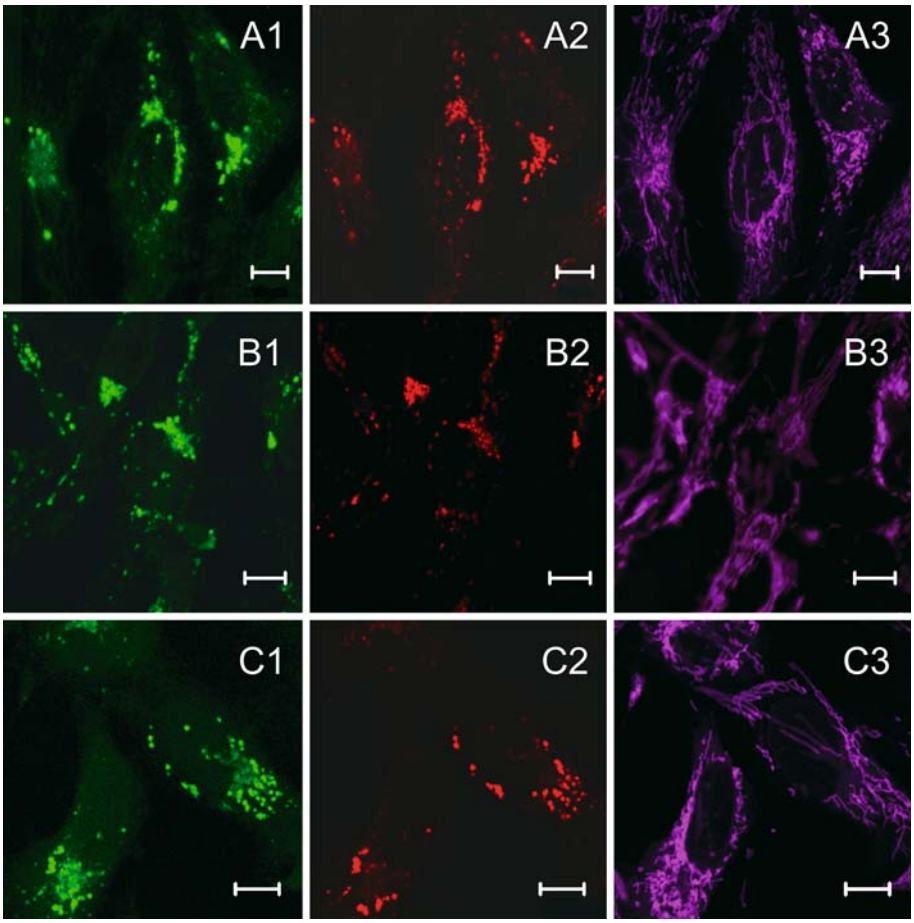

Figure 3. Subcellular localization of D11 labile zinc pools with organelle tracers. Cells were labelled simultaneously with labile zinc indicators and lysosome (LysoTracker Red DND99) or mitochondria-specific (MitoTracker Deep Red) probes and imaged as described in *Materials and Methods*. Row (a) BTC-5N (A1); LysoTracker Red DND 99 (A2); MitoTracker Deep Red (A3) / Row (b) FluoZin-3 (B1); LysoTracker Red DND99 (B2); MitoTracker Deep Red (B3) / Row (c) ZinPyr-1 (C1); LysoTracker Red DND99 (C2); MitoTracker Deep Red (C3). Confocal imaging was done with a 63× C-Apochromat water immersion objective. Scale bars (10 μM) are indicated.

in advance to be able to colocalize high fluorescence values with any known cell compartment. Our results clearly show that the punctuate zinc pools which contain the majority of labile zinc are traced by LysoTracker Red and therefore can be considered lysosomic bodies (Figure 3). In contrast, no correlation was seen between zinc labelling and mitochondria-specific staining. As shown in Figure 3, similar results were obtained for FluoZin-3, ZinPyr-1 or BTC-5N labelling.

Our preliminary work showed that FluoZin-3 has much better characteristics particularly in terms of dye retention and quantum yield; therefore we restricted further experiments to the use of FluoZin-3 to estimate labile zinc fluxes.

Extracellular zinc induces labile zinc fluxes in D11 cells

Exposure of D11 cells to 10 μM $ZnCl_2$ alone readily induced multiple local elevations of fluorescence intensity as shown in Figure 4a and b. This Zn concentration, although quite high, was not toxic to the cells, as determined in a 2 h cytotoxicity experiment using resazurin reduction as a viability marker (not shown). However, it allowed to observe clear changes in fluorescence within a short time frame. Subsequent co-application of sodium pyrithione (10 μM), a zinc ionophore, resulted in a sudden rise in the fluorescence signal which still appeared punctuate

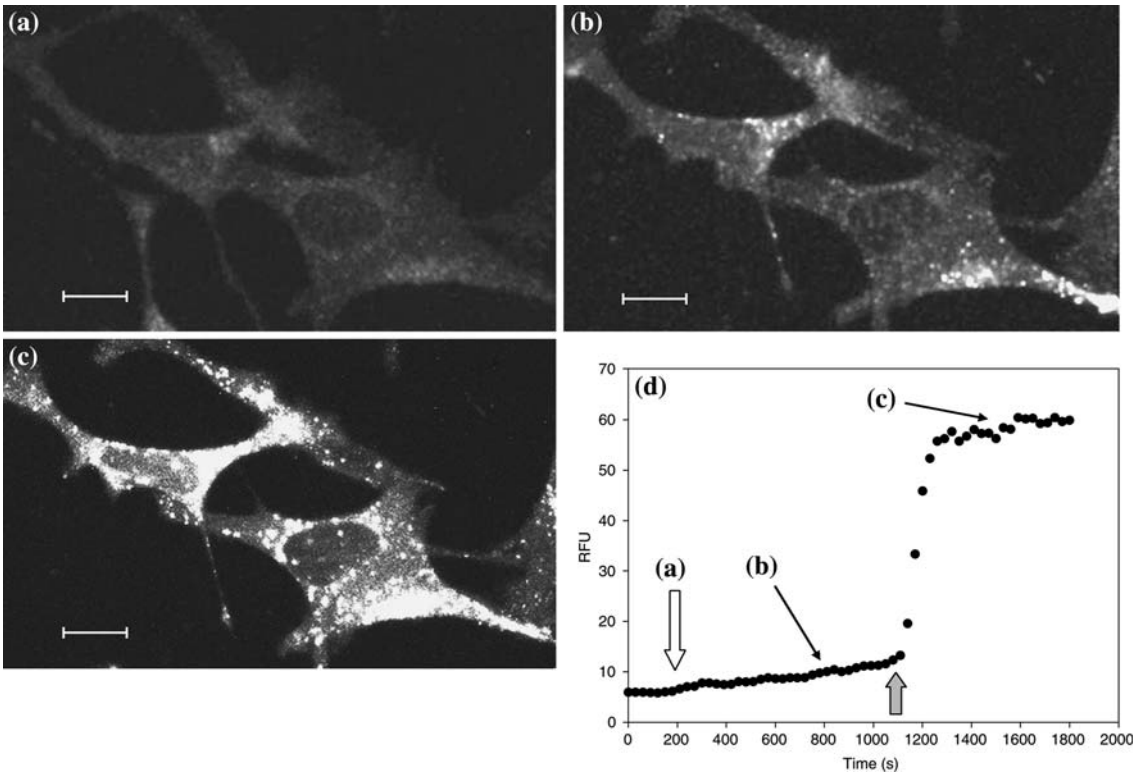

Figure 4. Response of D11 cells to extracellular zinc. After FluoZin-3 loading, cells were exposed to 10 μM $ZnCl_2$ and imaged (high magnification, 63× water immersion objective (C-Apochromat)) at time point 0 (a) just before and 10 min after (b) Zn triggering. To saturate FluoZin-3 with Zn^{2+} cells were subsequently incubated with pyrithione (10 μM) until a plateau phase was reached (c). Scale bars (10 μM) are indicated in the lower corners. Plot (d) shows the mean fluorescence trace of 3 individual cells selected as ROI (region of interest) and representative of 4 independent experiments. (RFU: relative fluorescence units).

and comparable to the use of $ZnCl_2$ alone (Figure 4c). However, at the same time we observed some sort of clustering of initially smaller pools into larger vesicular entities. Either with or without zinc permeabilization, nuclei did not show any significant response. Fig 4d shows the mean fluorescence trace during the experiment and highlights the fluorescence values corresponding to Figure 4a–c. Based upon the apparent maximum after zinc-pyrithione exposure and the minimum after chelation of probe-bound Zn(II) with TPEN (not shown), basal Zn^{2+} levels were estimated at 1.4 ± 0.2 nM (S.E.M., $n = 20$ cells), which increased to 9.5 ± 1.3 nM (S.E.M., $n = 20$ cells) after 30 min exposure to 10 μM $ZnCl_2$ (Figure 5).

Using an ionophore for zinc, we actually expected to obtain an even distribution of Zn^{2+} throughout the cell at equilibrium. Since 10-fold concentrations of Zn-pyrithione (100 μM each) yielded similar results (not shown), the exposure time was increased in separate experiments. Starting from low pre-exposure fluorescence levels (Figure 6a), vesicular saturation was attained in a burst-like phase (image not shown) but after 25 min fluorescence became more homogeneously distributed throughout the cytoplasm and nucleus (Figure 6b). Finally, a sudden loss of fluorescence after 120–140 min could be explained by the concomitant onset of cellular necrosis, as assessed using ethidium homodimer-1 (EtH-1) staining (Figure 6c). Typically, EtH-1 positive cells also contained some remaining FluoZin-3 fluorescence concentrated in a juxtanuclear spot but we could not establish whether this originated from coalescence of local zinc pools. Figure 6d outlines the time course of the initial fluorescence saturation and the subsequent slow kinetic component resulting in cytotoxicity, corresponding to Figure 6a–c.

Apparently, Zn^{2+} introduced in the hepatocytes by pyrithione, can be buffered temporarily in

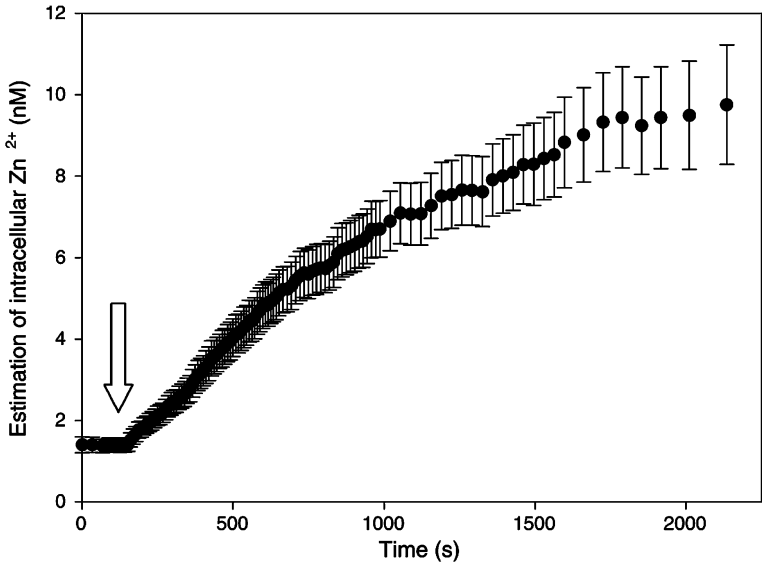

Figure 5. Quantified intracellular Zn^{2+} fluxes in D11 cells after exposure to 10 μM $ZnCl_2$. Responses of FluoZin-3 were calibrated by generating maximum and minimum fluorescence signals with Zn-pyrithione (10 μM) and TPEN (50 μM), respectively. Estimations were based on the general equation $[Zn^{2+}_i] = K_d \times (F - F_{min})/(F_{max} - F)$ with $K_{d(Zn)} = 15$ nM. Data points refer to the mean of 20 cells pooled out of 3 independent experiments. *Y*-axis bars represent S.E. of the mean.

the vesicular compartment until the regulatory mechanisms brake down, which finally results in toxic Zn(II) levels. Since the observations made with Na-pyrithione may be related specifically to this compound, we decided to also investigate the effects of another ionophore on cellular zinc fluxes.

D11 cells recover from temporary cytosolic zinc fluxes triggered with 4-Br A23187 by vesicular sequestration

Exposure of D11 hepatocytes to Zn-pyrithione did not allow us to demonstrate fluxes of cytosolic Zn^{2+} towards the vesicular compartment. As an alternative, we applied $ZnCl_2$ (10 μM) together with 4-Br A23187 (1 μM), a non-fluorescent ionophore for divalent cations among which Zn(II) (Canzoniero *et al*. 1999). Additionally, cells were pretreated with TPEN (50 μM, 10 min) to deplete labile zinc (Figure 7a). This measure facilitates time-dependent detection of fluorescence rises in any cellular compartment. In contrast to pyrithione exposure, 4-Br A23187 initially induced a general fluorescence increase in the cytoplasm but not in the nucleus or the vesicular compartment (Figure 7b). Confocal images captured 15 min after the start of exposure (Figure 7c) demonstrate the sequestration of cytosolic fluorescence into punctuate vesicles. However, overall cellular fluorescence levels did not appreciably change any further and an apparent plateau phase was present in the mean trace (Figure 7d). Remarkably, already at 35 min cells had returned back to original fluorescence levels (Figure 7d). At this stage, cells were still not permeable to EtH-1 (image not shown), which confirms their viability. Thus, a zinc permeabilization treatment with 4-Br A23187, in contrast with pyrithione, has clear transient effects on labile Zn(II) distribution in D11 cells. These results indicate that the vesicular compartment is involved in sequestration of labile Zn(II) from the cytoplasm, but its capacity is limited.

Intracellular zinc release also generates non-vesicular labile zinc

Most of the cellular zinc pool is tightly bound and since this fraction is presumably not available to fluorigenic zinc chelators such as FluoZin-3 ($K_{d(Zn)} \sim 15$ nM), generally low fluorescence values are to be expected. We applied NEM which alkylates intracellular sulfhydryl residues, in order to block these high-affinity binding sites. After a short lag phase ($\pm$3 min), 100 μM NEM induced an overall rise in cellular fluorescence (both cytosolic and nuclear) (Figure 8a, b) during the

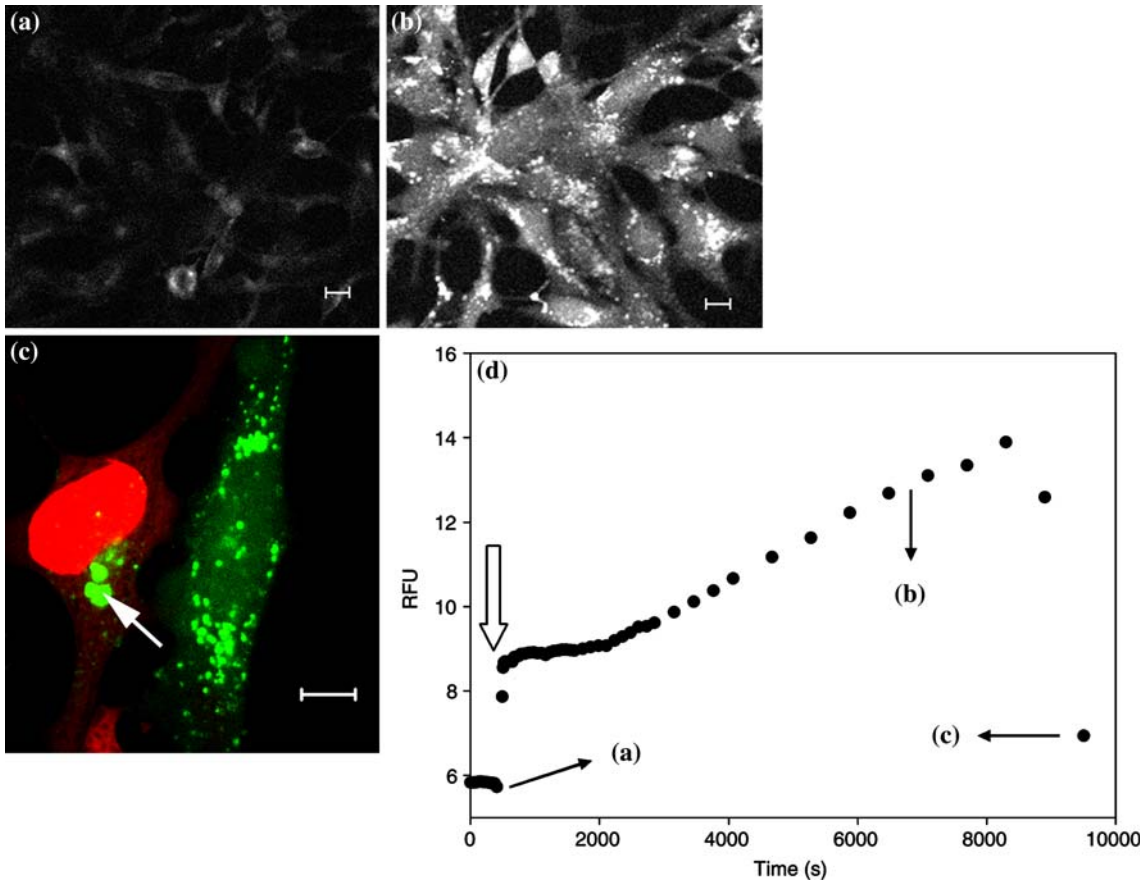

Figure 6. Time-dependent effect of Zn-pyrithione on intracellular labile zinc distribution. Panels shown are FluoZin-3 loaded D11 cells imaged at zero timepoint before exposure (a), and subsequently after 2 h (b) of $ZnCl_2$ + Na-pyrithione (each 10 μM) exposure. Image c displays a close-up (63× water-immersion objective) of 2 cells after staining with ethidium homodimer-1 (excitation: 543 nm, emission: BP 565–615 nm) at the end of the experiment (left: dead cell; white arrow points at perinuclear spot). Scale bars (10 μM) are indicated in the lower corners. Time points that match the respective panels a–c are shown in the mean fluorescence intensity plot (d) ($n = 20$–25 cells, representative of 3 independent experiments). In (d), the start of Zn-pyrithione exposure is indicated by an open arrow. (RFU: relative fluorescence units).

monitoring period (30 min). When zinc-pyrithione (10 μM of $ZnCl_2$ combined with equimolar Na-pyrithione) was applied subsequently, FluoZin-3 fluorescence was effectively activated to a maximum of its potential at 5 min (Figure 8c). This is also clear from the average cellular fluorescence plot shown in Figure 8d. Under these conditions, D11 cells displayed a bright fluorescence evenly distributed throughout the cytoplasm and nucleus. So by blocking important Zn^{2+} ligands it is possible to detect zinc pools previously inaccessible to the zinc sensor. Titration of cells with TPEN, a membrane-permeable heavy metal chelator ($K_{d(Zn)} \sim 10^{-16}$), removes all FluoZin-3 fluorescence; this confirms the high overall [Zn^{2+}] availability. When signal intensities induced by zinc-pyrithione and TPEN are now considered respectively as FluoZin-3 fluorescence maxima and minima, basal levels of labile zinc can be approximated at 0.5 ± 0.07 nM (S.E.M., $n = 20$ cells) which rise to about 3 ± 0.24 nM (S.E.M., $n = 20$ cells) after 30 min of exposure to NEM (Figure 9).

Discussion

We have shown that in the hepatic trout cell line D11, the most reactive (“chelatable”) zinc is localized in acidic compartments as traced by LysoTracker DND99, a dye which specifically accumulates in these compartments. Three fluorescent zinc probes with sub-μM affinity for Zn^{2+}

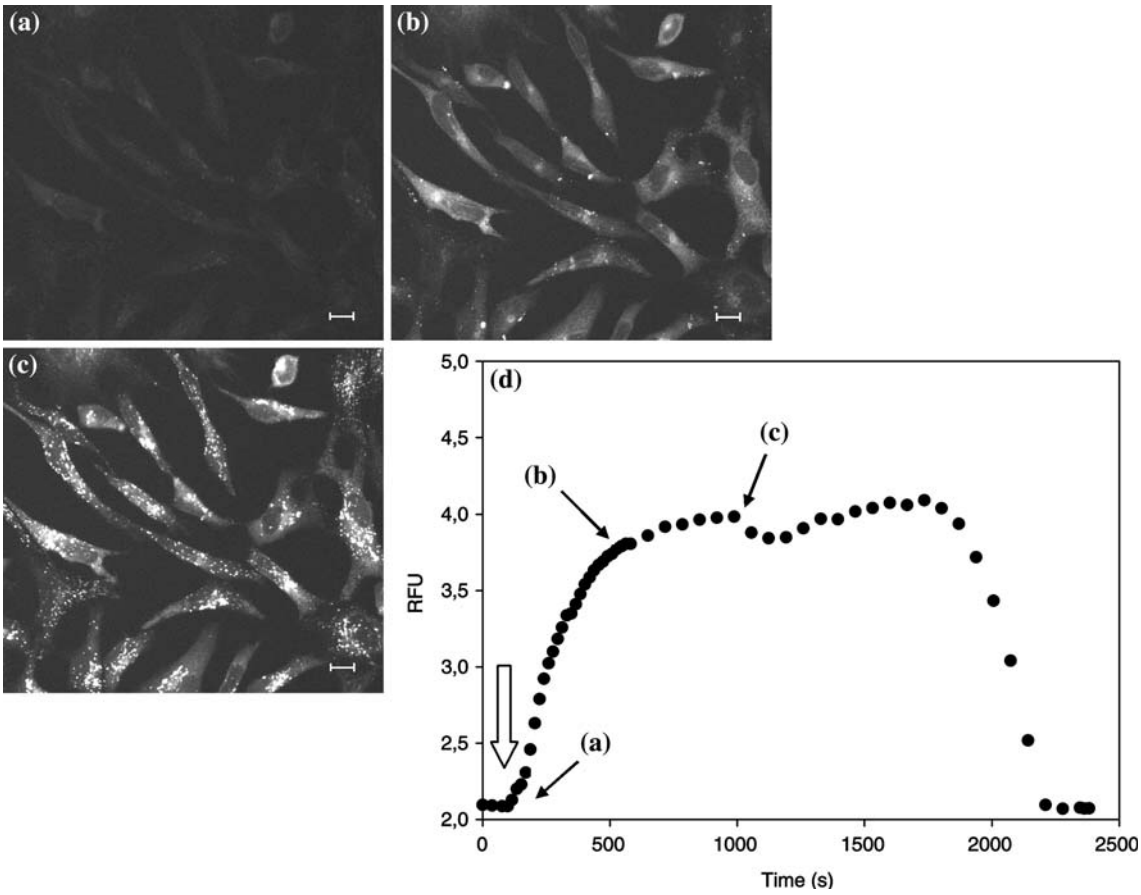

Figure 7. Combined effect of 4-Br-calcimycin (1 μM) and $ZnCl_2$ (10 μM) on labile zinc depleted D11 cells after 0 min (a), 5 min (b) and 15 min (c). Figure 7c shows highly fluorescent vesicles. Scale bars (10 μM) are indicated in the lower corners. Signal trace plotted in Figure 7d is based upon the calculated mean intensity values ($n = 20$–25 cells, 3 independent experiments) of the D11 cells imaged during the course of the experiment. White arrow in (d) indicates the trigger start and labels a–c refer to Figure 7a–c. (RFU: relative fluorescence units).

and a different chemical basis (ZinPyr-1, BTC-5N and FluoZin-3) allowed demonstrating co-localization of labile zinc and LysoTracker. So far no ZnT-type proteins have been described which are expressed in cultured liver cells and could be uniquely associated with the labile zinc pools observed in the D11 cell line. Intruigingly, a recent study on a novel ZIP-type protein, human BigM103, showed that this protein colocalizes with a Lysotracker-positive compartment and affects Zn^{2+} levels as measured by Newport Green, another fluorescent zinc sensor (Begum *et al.* 2002).

Our results with FluoZin-3 show that this zinc sensor is able to reveal the vesicular nature of Zn(II) in eukaryotic cells. Moreover, it appears to be well suited to monitor time-dependent intracellular fluxes in cultured trout liver cells. We have induced Zn(II) fluxes in different ways. Firstly, after exposure to 10 μM of extracellular zinc, Zn(II) is taken up in local pools without appearing in a probe-available (''chelatable'') form in the bulk cytoplasm. Sodium pyrithione, a commonly used zinc ionophore, induces maximal fluorescence levels in combination with $ZnCl_2$, but these are limited to acidic (endosomal) compartments on a short term. Correspondingly, when applied on neuronal cells, Zn-pyrithione saturates only vesicular zinc, even at higher concentrations (Ho *et al.* 2000). However, application of 4-Br A23187 revealed the presence of temporary cytosolic Zn fluxes before redistribution to the vesicles. Finally, *N*-ethylmaleimide is able to gradually release zinc from sulfhydryl residues, which leads to a general fluorescence increase throughout the cell and homogenous saturation of FluoZin-3 upon

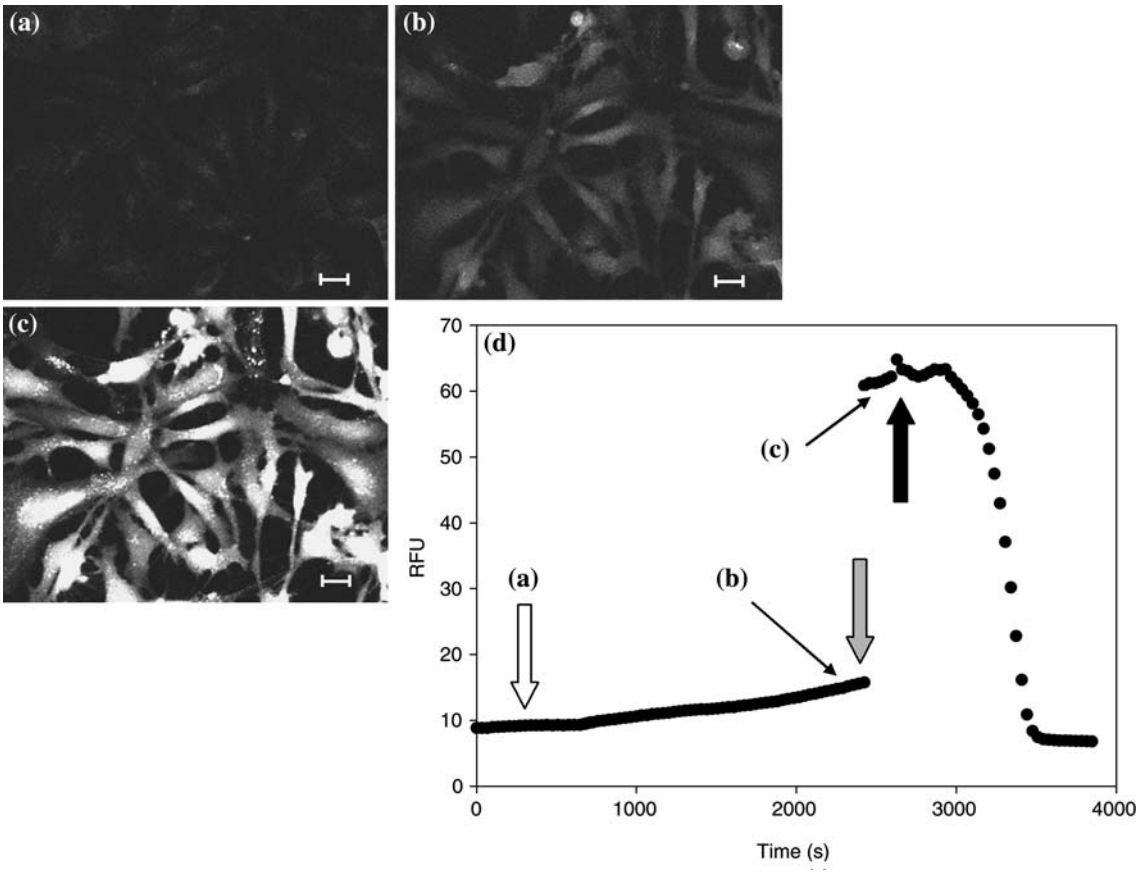

Figure 8. Fluorescent response (Ar excitation 488 nm – emission BP 500–530 nm) of FluoZin-3 loaded D11 cells (a) after 35 min exposure to 100 μM NEM (b), subsequent triggering with $ZnCl_2$ (10 μM) plus Na-pyrithione (10 μM) (c) and during TPEN (50 μM) washing (image not shown). Scale bars (10 μM) are indicated in the lower corners. Arrows in (d) mark the start of different treatments: NEM (open arrow); Zn-pyrithione (gray arrow); TPEN (black arrow). Plotted results shown in Figure 8d represent the mean cellular intensity values ($n = 25$–30 cells, representative of 3 independent experiments) of the cell field during the recorded time series. Labels a–c in Figure 8d correspond to the respective confocal images shown in Figure 8a–c.

subsequent Zn-pyrithione exposure. This agrees well with the observation that the disulfide oxidant DTDP (2, 2'-dithiopyridine) evokes detectable zinc fluxes in FluoZin-3 loaded neurons (Sensi *et al.* 2003a). Zinc release from MT clusters is of physiological relevance for its distribution, which means there is a rationale behind the use of oxidants and sulfhydryl blockers as a model for Zn(II) release in cells (Maret 2003). A working model for Zn^{2+} homeostasis was recently proposed (Colvin *et al.* 2003), which clearly positions MTs, zinc transporters as well as labile zinc. It provides a state-of-the-art framework for the study of zinc management in neuronal cells, but remains general enough to be applied to other cell types such as the fish hepatocytes studied here.

Perspectives for quantification of [Zn^{2+}] fluxes using FluoZin-3

Clamping minimum and maximum fluorescence signals by using equilibration with ionophores and metal chelators seems a straightforward approach to derive Zn^{2+} levels, but results must be interpreted with caution. Our experiments demonstrate that mean fluorescence intensities should not be the only basis to interpret ion fluxes in probed cells. Using confocal laser scanning microscopy sufficient spatial resolution can be provided to uncover subcellular fluorescence patterns. For example, we showed that generating intracellular conditions to saturate FluoZin-3 homogenously in D11 cells is not always feasible. In contrast, Haase

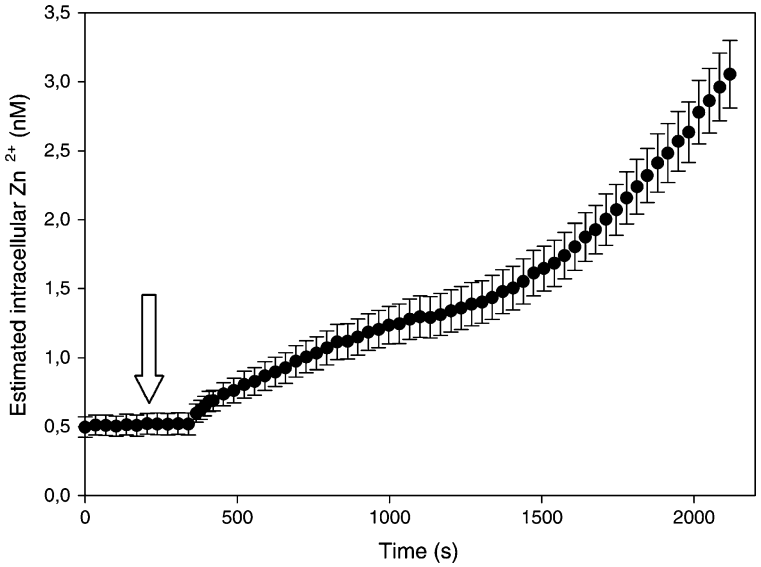

Figure 9. Changes in intracellular $[Zn^{2+}]$ after exposure of D11 cells to 100 μM NEM. Calibration of FluoZin-3 signals was performed at the end of NEM exposure by inducing maximum and minimum fluorescence signals with Zn-pyrithione (10 μM) and TPEN (50 μM), respectively. Calculations are based upon the general equation $[Zn^{2+}{}_i] = K_d \times (F - F_{min})/(F_{max} - F)$ with $K_{d(Zn)} = 15$ nM. Data points refer to the mean of 25 cells pooled out of 3 independent experiments. Y-axis bars mark mean ± S.E.M.

& Beyersmann (2002) reported an even distribution of Zinquin fluorescence in C6 glioma cells after Zn-pyrithione treatment. Maximum total cell fluorescence could easily be generated after NEM exposure while 10 μM Zn-pyrithione only induced local maxima after $ZnCl_2$ exposure of D11 hepatocytes. This may be due to the very efficient buffering of endogenous metals like Zn. NEM can affect Zn (II) homeostasis drastically by causing direct inactivation of MTs and GSH, two important metal chelators (Maracine & Segner 1998; Shaw *et al*. 1997). Eventually NEM can interfere with any possible component of the Zn transport process, such as vesicular trafficking or transporter function (Glover & Hogstrand 2002). Apparently our results contrast with the findings of Haase and Beyersmann (2002) who observed a transient rise of vesicular free Zn(II) in C6 cells, minutes after NEM exposure. Since experiments with other cell lines were more in line with our observations, we suspect that this phenomenon may be cell-type dependent. Nevertheless, treatment of D11 cells with NEM is likely to shift cellular Zn buffering to conditions that favour the accumulation of Zn(II) species chelatable by FluoZin-3.

In the present study, quantitative results obtained by performing an ionophore calibration procedure after $ZnCl_2$ exposure solely refer to the vesicular pool. In contrast, calculated $[Zn^{2+}]$ changes upon NEM exposure reflect fluxes in the entire cellular space. It should be clear that both have to be interpreted in an entirely different physiological context. Apart from its correct biophysical interpretation many other potential error sources in labile Zn^{2+} estimation exist, e.g. ignoring differences in subcellular Zn^{2+}-FluoZin-3 affinity and intrinsic fluorescence yields. Clearly, measurements of Zn^{2+} should only be compared when ion fluxes during experimental exposures and the calibration procedure refer to the same subcellular compartments. Moreover, due to variations in instrumental and experimental parameters single-wavelength probes are still inferior to two-wavelength sensors which allow ratiometric measurements (Chang *et al*. 2004).

An important warning concerning cellular Zn^{2+} quantification came from Dineley and coworkers (2002) who pointed out that Zn probes introduced by their ester form are likely to accumulate to a level where they participate in cellular Zn buffering (several mM). This can explain why Zn indicators with a different affinity can appear equally sensitive to Zn^{2+}. Also, this may be part of the reason why reported free Zn(II) levels differ several orders of magnitude, for example 10^{-6} M of free Zn^{2+} measured with Zinquin in freshly

isolated rat hepatocytes (Kleineke & Brand 1997) or 10^{-9} M of free Zn^{2+} in rabbit myocytes (Turan *et al.* 1997), with fura-2. Since the total intracellular probe concentration is a poorly accessible factor, absolute interpretations of calculated free Zn^{2+} levels must be avoided (Dineley *et al.* 2002).

In conclusion, fluorescent Zn probes can be useful to unravel the physiology of Zn(II) in trout liver cells. Under normal physiological conditions the bulk cytosolic and nuclear Zn^{2+} is not detectable with FluoZin-3, therefore they represent sub-nM levels. Using FluoZin-3 labelled trout hepatocytes we have directly demonstrated two properties of the intracellular Zn homeostasis:

1. Endosomal pools contribute to the buffering of cytosolic zinc fluxes and there is a dynamic interaction between these two compartments.
2. Thiolate ligands have a first-line involvement in controlling available intracellular Zn(II).

Recently, RhodZin-3, a derivative of FluoZin-3 which is specifically retained in mitochondria, has been synthesized and evaluated in neurons (Sensi *et al.* 2003a; Sensi *et al.* 2003b). In the perspective of our results, it would be highly desirable to extend this approach to the design of Zn probes targeted to specific endosomal and other compartments.

Acknowledgements

The authors wish to thank J. Van Daele for his support in the confocal microscopy work and Dr. J. Robbens for revision of the manuscript and constructive criticism.

References

Ahne W. 1985 Studies on the use of fish tissue-cultures for toxicity tests in order to reduce and replace the fish tests. *Zentralbl Bakteriol Mikrobiol Hyg B* **180**, 480–504.

Alsop DH, Wood CM. 2000 Kinetic analysis of zinc accumulation in the gills of juvenile rainbow trout: effects of zinc acclimation and implications for biotic ligand modeling. *Environ Toxicol Chem* **19**, 1911–1918.

Arslan P, Divirgilio F, Beltrame M, Tsien RY, Pozzan T. 1985 Cytosolic Ca-2^{+} homeostasis in Ehrlich and Yoshida carcinomas – A new, membrane-permeant chelator of heavy metals reveals that these ascites tumor cell lines have normal cytosolic free $Ca2^{+}$. *J Biol Chem* **260**, 2719–2727.

Begum NA, Kobayashi M, Moriwaki Y, *et al.* 2002 Mycobacterium bovis BCG cell wall and lipopolysaccharide induce a novel gene, BIGM103, encoding a 7-TM protein: Identification of a new protein family having Zn-transporter and Zn-metalloprotease signatures. *Genomics* **80**, 630–645.

Brand IA, Kleineke J. 1996 Intracellular zinc movement and its effect on the carbohydrate metabolism of isolated rat hepatocytes. *J Biol Chem* **271**, 1941–1949.

Burdette SC, Walkup GK, Spingler B, Tsien RY, Lippard SJ. 2001 Fluorescent sensors for Zn^{2+} based on a fluorescein platform: Synthesis, properties and intracellular distribution. *J Am Chem Soc* **123**, 7831–7841.

Bury NR, Walker PA, Glover CN. 2003 Nutritive metal uptake in teleost fish. *J Exp Biol* **206**, 11–23.

Canzoniero LMT, Turetsky DM, Choi DW. 1999 Measurement of intracellular free zinc concentrations accompanying zinc-induced neuronal death. *J Neurosci* **19**, RC31.

Chang CJ, Jaworski J, Nolan EM, Sheng M, Lippard SJ. 2004 A tautomeric zinc sensor for ratiometric fluorescence imaging: Application to nitric oxide-induced release of intracellular zinc. *Proc Natl Acad Sci USA* **101**, 1129–1134.

Colvin RA, Fontaine CP, Laskowski M, Thomas D. 2003 Zn^{2+} transporters and Zn^{2+} homeostasis in neurons. *Eur J Pharmacol* **479**, 171–185.

Coyle P, Zalewski PD, Philcox JC, *et al.* 1994 Measurement of zinc in hepatocytes by using a fluorescent probe, Zinquin: Relationship to metallothionein and intracellular zinc. *Biochem J* **303**, 781–786.

Dineley KE, Malaiyandi LM, Reynolds IJ. 2002 A reevaluation of neuronal zinc measurements: Artifacts associated with high intracellular dye concentration. *Mol Pharmacol* **62**, 618–627.

Frederickson CJ, Kasarskis EJ, Ringo D, Frederickson RE. 1987 A quinoline fluorescence method for visualizing and assaying the histochemically reactive zinc (bouton zinc) in the brain. *J Neurosci Methods* **20**, 91–103.

Gagné F, Blaise C. 1996 Available intracellular Zn as a potential indicator of heavy metal exposure in rainbow trout hepatocytes. *Environ Toxicol Water Qual* **11**, 319–325.

Gaither LA, Eide DJ. 2001 Eukaryotic zinc transporters and their regulation. *Biometals* **14**, 251–270.

Glover CN, Hogstrand C. 2002 In vivo characterisation of intestinal zinc uptake in freshwater rainbow trout. *J Exp Biol* **205**, 141–150.

Grynkiewicz G, Poenie M, Tsien RY. 1985 A new generation of Ca^{2+} indicators with greatly improved fluorescence properties. *J Biol Chem* **260**, 3440–3450.

Haase H, Beyersmann D. 2002 Intracellular zinc distribution and transport in C6 rat glioma cells. *Biochem Biophys Res Commun* **296**, 923–928.

Haugland R. 2002 Handbook of Fluorescent Probes and Research Products. La Jolla: Molecular Probes.

Ho LH, Ratnaike RN, Zalewski PD. 2000 Involvement of intracellular labile zinc in suppression of DEVD-caspase activity in human neuroblastoma cells. *Biochem Biophys Res Commun* **268**, 148–154.

Hogstrand C, Wood CM. 1995 Mechanisms for zinc acclimation in fresh-water rainbow-trout. *Mar Environ Res* **39**, 131–135.

Hogstrand C, Wood CM. 1996 The physiology and toxicology of zinc in fish. In: Tayler EW, ed., *Toxicology of Aquatic Pollution: Physiological, Cellular and Molecular Approaches.* Cambridge: Cambridge University Press, pp. 61–84.

Kägi JHR. 1991 Overview of metallothionein. *Methods Enzymol* **205**, 613–626.

Kambe T, Yamaguchi-Iwai Y, Sasaki R, Nagao M. 2004 Overview of mammalian zinc transporters. *Cell Mol Life Sci* **61**, 49–68.

Kleineke JW, Brand IA. 1997 Rapid changes in intracellular Zn^{2+} in rat hepatocytes. *J Pharmacol Toxicol Methods* **38**, 181–187.

Krezel A, Wojcik J, Maciejczyk M, Bal W. 2003 May GSH and L-His contribute to intracellular binding of zinc? Thermodynamic and solution structural study of a ternary complex. *Chem Commun*, 704–705.

Ley HL, Failla ML, Cherry DS. 1983 Isolation and characterization of hepatic metallothionein from rainbow trout (*Salmo gairdneri*). *Comp Biochem Physiol B* **74**, 507–513.

Lopez-Garcia C, Varea E, Palop JJ, *et al*. 2002 Cytochemical techniques for zinc and heavy metals localization in nerve cells. *Microsc Res Tech* **56**, 318–331.

Maracine M, Segner H. 1998 Cytotoxicity of metals in isolated fish cells: Importance of the cellular glutathione status. *Comp Biochem Physiol A* **120**, 83–88.

Maret W. 2003 Cellular zinc and redox states converge in the metallothionein/thionein pair. *J Nutr* **133**, 1460S–1462S.

Michalczyk AA, Allen J, Blomeley RC, Ackland ML. 2002 Constitutive expression of hZnT4 zinc transporter in human breast epithelial cells. *Biochemical J* **364**, 105–113.

Nasir MS, Fahrni CJ, Suhy DA, *et al*. 1999 The chemical cell biology of zinc: structure and intracellular fluorescence of a zinc-quinolinesulfonamide complex. *J Biol Inorg Chem* **4**, 775–783.

Outten CE, O'Halloran TV. 2001 Femtomolar sensitivity of metalloregulatory proteins controlling zinc homeostasis. *Science* **292**, 2488–2492.

Palmiter RD, Cole TB, Findley SD. 1996a ZnT-2, a mammalian protein that confers resistance to zinc by facilitating vesicular sequestration. *Embo J* **15**, 1784–1791.

Palmiter RD, Cole TB, Quaife CJ, Findley SD. 1996b ZnT-3, a putative transporter of zinc into synaptic vesicles. *Proc Natl Acad Sci USA* **93**, 14934–14939.

Pierson KB. 1985 Occurrence and synthesis of a non-thionein, zinc-binding protein in the rainbow-trout (*Salmo gairdneri*). *Comp Biochem Physiol C* **81**, 71–75.

Qiu A, Shayeghi M, Hogstrand C. 2005 Molecular cloning and functional characterization of a high-affinity zinc importer (DrZIP1) from zebrafish (Danio rerio). *Biochem J* **388**, 745–754.

Ranaldi G, Perozzi G, Truong-Tran A, Zalewski P, Murgia C. 2002 Intracellular distribution of labile Zn(II) and zinc transporter expression in kidney and MDCK cells. *Am J Physiol* **283**, F1365–F1375.

Salguiero MJ, Zubillaga M, Lysionek A, *et al*. 2000 Zinc as an essential micronutrient: A review. *Nutr Res* **20**, 737–755.

Sauer GR, Watabe N. 1989 Ultrastructural and histochemical aspects of zinc accumulation by fish scales. *Tissue & Cell* **21**, 935–943.

Sensi SL, Ton-That D, Sullivan PG, *et al*. 2003a Modulation of mitochondrial function by endogenous Zn^{2+} pools. *Proc Natl Acad Sci USA* **100**, 6157–6162.

Sensi SL, Ton-That D, Weiss JH, Rothe A, Gee KR. 2003b A new mitochondrial fluorescent zinc sensor. *Cell Calcium* **34**, 281–284.

Shaw CF, He LB, Munoz A, *et al*. 1997 Kinetics of reversible *N*-ethylmaleimide alkylation of metallothionein and the subsequent metal release. *J Biol Inorg Chem* **2**, 65–73.

Tang ZL, Wasserloos KJ, Liu XH, *et al*. 2002 Nitric oxide decreases the sensitivity of pulmonary endothelial cells to LPS-induced apoptosis in a zinc-dependent fashion. *Mol Cell Biochem* **234**, 211–217.

Turan B, Fliss H, Desilets M. 1997 Oxidants increase intracellular free Zn^{2+} concentration in rabbit ventricular myocytes. *Am J Physiol* **41**, H2095–H2106.

Vallee BL, Falchuk KH. 1993 The biochemical basis of zinc physiology. *Physiol Rev* **73**, 79–118.

Zalewski PD, Forbes IJ, Betts WH. 1993 Correlation of apoptosis with change in intracellular labile Zn(II) using Zinquin [(2-methyl-8-P-toluenesulphonamido-6-quinolyl-oxy)acetic acid], a new specific fluorescent-probe for Zn(II). *Biochem J* **296**, 403–408.